Electrical properties and colossal electroresistance of heteroepitaxial $SrRuO_3/SrTi_{1-x}Nb_xO_3$ ($0.0002 \leqslant x \leqslant 0.02$) Schottky junctions

T. Fujii and M. Kawasaki
Correlated Electron Research Center (CERC), National Institute of Advanced Industrial Science and Technology (AIST), Tsukuba, Ibaraki 305-8562, Japan
and Institute for Materials Research, Tohoku University, Sendai 980-8577, Japan

A. Sawa*
Correlated Electron Research Center (CERC), National Institute of Advanced Industrial Science and Technology (AIST), Tsukuba, Ibaraki 305-8562, Japan

Y. Kawazoe
Institute for Materials Research, Tohoku University, Sendai 980-8577, Japan

H. Akoh
Correlated Electron Research Center (CERC), National Institute of Advanced Industrial Science and Technology (AIST), Tsukuba, Ibaraki 305-8562, Japan
and CREST-JST, Kawaguchi, Saitama 322-0012, Japan

Y. Tokura
Correlated Electron Research Center (CERC), National Institute of Advanced Industrial Science and Technology (AIST), Tsukuba, Ibaraki 305-8562, Japan
and Department of Applied Physics, University of Tokyo, Tokyo 113-8658, Japan

(Received 14 November 2006; revised manuscript received 1 February 2007; published 2 April 2007)

We investigated the electrical properties of heteroepitaxial oxide Schottky junctions, $SrRuO_3/SrTi_{1-x}Nb_xO_3$ ($0.0002 \leqslant x \leqslant 0.02$). The overall features agree with those of a conventional semiconductor Schottky junction, as exemplified by the rectifying current (I)-voltage (V) characteristics with linear $\log I$-V relationship under forward bias and the capacitance (C)-V characteristics with linear $1/C^2$-V relationship under reverse bias. The x dependence of the junction parameters, such as barrier height, built-in potential, and depletion layer width, can be analyzed by taking into account the band-gap narrowing due to degeneration, as well as the bias-dependent dielectric constant of depleted $SrTiO_3$. All junctions, except for the most heavily doped ($x=0.02$) one, show hysteretic I-V characteristics with a colossal electroresistance (CER) effect, where forward (reverse) bias stress reduces (enhances) the junction resistance. The x dependence of the CER effect and the absence of hysteresis in the C-V relationship suggest that the resistance switching in Schottky junctions comes from the change in conductance through additional tunneling paths rather than the change in barrier potential profile. Electron charging in or discharging from a self-trap depending on the bias polarity may account for the nonvolatility of the CER effect. This model is supported by the fact that the CER effect is completely suppressed in interface-engineered junctions with a $SrRuO_3$/2-nm-thick $X/SrTi_{0.99}Nb_{0.01}O_3$ structure, where X is either pristine $SrTiO_3$ or very heavily electron-doped $La_{0.25}Sr_{0.75}TiO_3$.

DOI: 10.1103/PhysRevB.75.165101 PACS number(s): 77.90.+k, 73.40.−c, 73.30.+y

I. INTRODUCTION

Perovskite oxides exhibit a wide variety of interesting physical properties, such as high-T_C superconductivity, colossal magnetoresistance, and charge and orbital ordering.[1] Recently, there has been a considerable deal of interest in electric-field- and/or current-induced nonvolatile resistance switching phenomena in such materials at room temperature. The so-called colossal electroresistance (CER) effect has been found in capacitorlike structures with various insulating oxides, such as Cr-doped $SrZrO_3$,[2] $SrTiO_3$,[3] and $Pr_{0.7}Ca_{0.3}MnO_3$ (PCMO),[4] sandwiched by two metal electrodes. Integrated circuits of nonvolatile resistance random access memories based on the CER effect have been demonstrated with PCMO,[5] NiO,[6] and Cu_xO (Ref. 7) as active layers. Although the CER effect has been extensively studied, both experimentally and theoretically,[8–27] the precise mechanism involved is not yet understood.

The CER effect reported so far can be classified into two types according to the difference in conducting path. One is the interface type, in which the CER effect takes place at the interface between metal electrodes and insulating (or semiconducting) oxides, where the contact resistance is changed by the application of an electric field at the interface.[8–15] The other is the filament type, in which the CER effect originates from the formation and rupture of conductive filaments in insulating oxides.[6,16–21] In the former case, the junction conductance is proportional to the junction area,[15] whereas in the latter case, the junction conductance is much less dependent on the junction area.[6,16] There is another way to categorize

the CER effect according to the resistance switching mode, i.e., bipolar or nonpolar types. Bipolar-type devices show directional resistance switching depending on the polarity of the applied voltage, which is the case for many perovskite oxide devices.[2–4,8–15,21] In contrast, in nonpolar-type devices, the resistance switching direction depends on the amplitude of the applied voltage, but not on the polarity.[6,16–20] This resistance switching mode has usually been observed in the filament-type CER effect.

The central issue is the origin of bistability in resistance and the driving mechanism involved in switching between the two resistance states. Reflecting the various types of materials used and CER effects observed, the proposed origins of the CER effect extend to electrochemical migration of oxygen ions,[8,9,22] a charging effect of the Schottky-like interface,[10–12] and a Mott transition induced by carrier doping[23–25] for the interface-type CER efffect, and electrochemical migration of oxygen ions,[21] Joule heating,[16] anodization,[20] and Mott transition[19,24,25] for the filament-type CER effect. Therefore, it is not practical to discuss the origin without detailed knowledge of the junction characteristics, the material parameters, and the device design.

We have previously proposed a possible scenario for the CER effect in perovskite oxide junctions, which is categorized as an interface type: a charging effect at Schottky junctions formed at one of the metal/insulator interfaces.[10–12] The experiments were carried out for Ti/PCMO (Ref. 10) and $SrRuO_3$ (SRO)/$SrTi_{1-x}Nb_xO_3$ (Nb:STO,[11] $x=0.01$) structures, where PCMO and Nb:STO were considered to form *p*-type and *n*-type Schottky junctions, respectively. These junctions show rectifying current-voltage (*I-V*) characteristics with a large hysteresis. Application of voltage pulses with forward or reverse polarities drives the junction to low or high resistance states, respectively, in a reversible fashion. Among these junctions, the SRO/Nb:STO junction is expected to be a suitable system for elucidating the mechanism of the CER effect because the SRO film can be pseudomorphically grown on an Nb:STO lattice, resulting in a well-defined interface.[11] Use of such a well-defined interface may enable us to reveal the intrinsic transport properties of the oxide Schottky junctions. The relationship between the CER effect and the electronic structure at the interface can be elucidated through systematic experimental studies on the junctions, such as the doping level dependence of the transport properties.

In this paper, we show that the CER effect can be seen for a wide range of *n*-type doping concentrations $0.0002 \leqslant x \leqslant 0.01$ in the SRO/Nb:STO junctions. The doping dependencies of the Schottky junction properties agree well with those of the conventional semiconductor model. However, if we insert nondoped or heavily doped layers as thin as five unit cells (2 nm), the CER effect disappears. Therefore, the CER effect should originate from an effect existing at the interface, and the appearance of the CER effect requires an appropriate donor concentration at the interface. On the other hand, the capacitance-voltage (*C-V*) characteristics do not show hysteretic behavior, unlike the hysteretic *I-V* characteristics. Based on these experimental results, we devise a model involving the opening and closing of resonant tunneling paths due to the charging effect at the interface as the origin of the CER effect for the heteroepitaxial junctions.

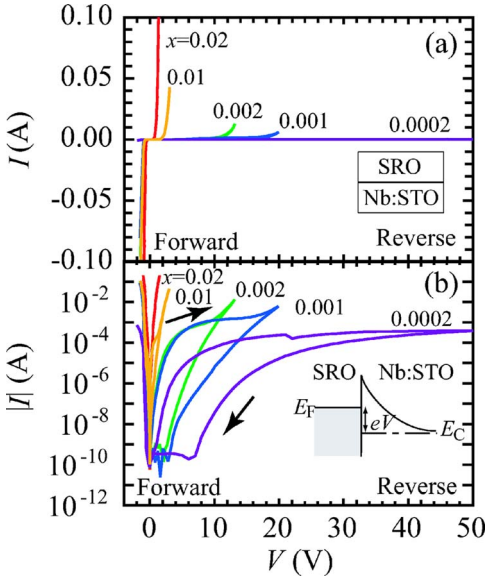

FIG. 1. (Color online) *I-V* characteristics of $SrRuO_3/SrTi_{1-x}Nb_xO_3$ (Nb:STO; $x=0.0002$, 0.001, 0.002, 0.01, and 0.02) junctions. (a) and (b) are plotted in linear and logarithmic current scales, respectively. The bias voltage was swept as $0 \rightarrow +V_{max} \rightarrow 0 \rightarrow -V_{max} \rightarrow 0$. The *I-V* characteristics show rectifying properties agreeing with that of conventional *n*-type semiconductor Schottky diode with a deep-work-function metal [see the band diagram of inset in (b) under reverse bias]. Large hysteresis is seen in the reverse-bias region except for the $x=0.02$ junction. The forward-bias *I-V* characteristics are magnified in Fig. 2.

II. EXPERIMENTAL PROCEDURES

The SRO/Nb:STO structures were prepared by pulsed laser deposition of epitaxial SRO (100 nm) films on (001) Nb:STO ($x=0.0002$, 0.001, 0.002, 0.01, and 0.02) single-crystal substrates at 650 °C in a 100 mTorr oxygen atmosphere. The doping level x in the Nb:STO substrates from a commercial source was confirmed by inductively coupled plasma emission spectrometry. Four-circle x-ray analysis revealed that the SRO films had identical in-plane lattice constant to that of the Nb:STO substrate (0.3905 nm), and the out-of-plane lattice constant was expanded to 0.395 nm.[28] The full-width at half maximum of the rocking curve for the (002) SRO peak was as narrow as 0.04°. The SRO surface exhibited a step-and-terrace structure as confirmed by atomic force microscopy.

Gold films (300 nm) were *ex situ* deposited on the SRO by electron-beam evaporation. The films were patterned into mesastructures with dimensions 100×100 μm^2 by conventional photolithography and Ar-ion etching. The *I-V* and *C-V* characteristics were measured by a two-probe method at 300 K, where positive bias was defined as the current flow from the Nb:STO to the SRO. The sample structure and the measurement configuration have been described in detail elsewhere.[11]

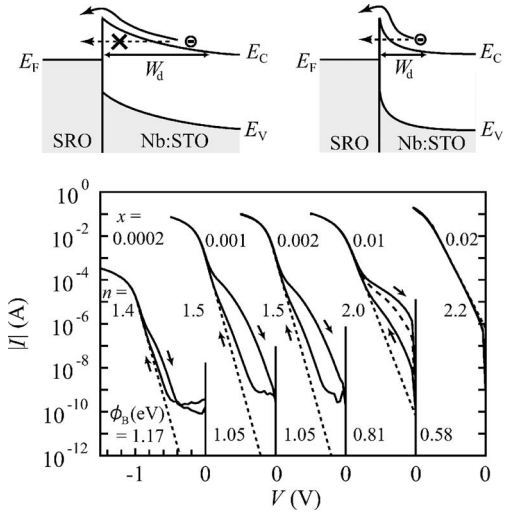

FIG. 2. Doping concentration dependence of forward-bias *I-V* characteristics for the $SrRuO_3/SrTi_{1-x}Nb_xO_3$ (Nb:STO; $x=0.0002$, 0.001, 0.002, 0.01, and 0.02) junctions. The broken straight lines are fits to the thermionic emission process. The voltage ranges of the fit are 0.8–1.0 V for the $x=0.0002$ and 0.001 junctions, 0.9–1.1 V for the $x=0.002$ junction, 0.8–1.0 V for the $x=0.01$ junction, and 0.5–0.7 V for the $x=0.02$ junction. From the fit, the ideality factor (n) and barrier height (ϕ_B) can be deduced. Considerable deviation is seen from the fit at lower bias voltage, representing excess current. Hysteretic behavior is seen only in this region. The schematic diagrams at the top illustrate possible band diagrams with light (left) and heavy (right) doping. The narrower barrier width in heavily doped junctions should promote a higher tunneling conduction contribution, giving rise to the excess current.

III. RESULTS AND DISCUSSIONS

A. *I-V* characteristics

Figure 1(a) shows *I-V* characteristics of the SRO/Nb:STO junctions with various doping levels x. All of the junctions show rectifying *I-V* characteristics consistent with those of a Schottky junction composed of n-type semiconductor and deep-work-function metal. As seen in Fig. 1(b), most of the junctions, except for the most heavily doped one ($x=0.02$), show *I-V* characteristics with large hysteresis. Here, we define the upper and lower branches of the *I-V* curve as a low-resistance state (LRS) and a high-resistance state (HRS), respectively. The resistance is switched from the LRS to the HRS by applying reverse (positive bias) stress. The magnified *I-V* characteristics under forward (negative) bias are shown in Fig. 2. By applying forward (negative) bias stress, the HRS is converted to the LRS.

If we take a standard semiconductor Schottky barrier model into account, I under forward bias is expressed as a function of V as

$$I = J_0 S \exp\left(\frac{eV}{nk_BT}\right), \tag{1}$$

$$J_0 = A^* T^2 \exp\left(-\frac{e\phi_B}{k_BT}\right), \tag{2}$$

where S is the junction area, e the electron charge, n an ideality factor, k_B Boltzmann's constant, T the temperature,

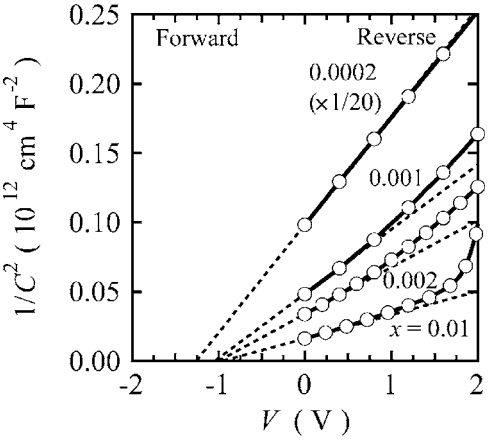

FIG. 3. *C-V* characteristics of the $SrRuO_3/SrTi_{1-x}Nb_xO_3$ (Nb:STO; $x=0.0002$, 0.001, 0.002, and 0.01) junctions. Because of leakage, reliable measurement could not be performed for the $x=0.02$ junction. More heavily doped junctions showed slight deviation from the straight line at high-bias voltage V due to the electric-field dependence of ε_S in Nb:STO, as well as the leakage current. The extrapolation of the straight broken lines to $1/C^2=0$ gives the built-in potential V_{bi} (for values, see Fig. 5).

A^* Richardson's constant, and ϕ_B the Schottky barrier height.[29] Therefore, I is expected to increase exponentially with V due to reduced $\phi_B - V$, which facilitates the thermionic emission process. In the higher V region prior to the saturation of I due to series Ohmic resistance, the log *I-V* characteristics fit well with the straight dotted lines. From the slopes of the straight lines, n can be determined, and from the intersection of I at $V=0$, ϕ_B can be determined, as shown in Fig. 2. As the doping level x increases, n is constant at about 1.5 for $x \leqslant 0.002$, and then increases above $x=0.01$, as also shown in Fig. 2. The increase in n close to or above 2 in junctions with heavier doping means that other current components increase in addition to the thermionic current. This can be understood from the opening of a parallel tunneling conduction channel at heavier doping due to the reduced barrier width, as shown schematically in illustrations at the top of Fig. 2. Because of the increase in tunneling current, the apparent ϕ_B decreases at heavier doping.

A deviation of the log *I-V* curves from the linear relationship can be seen at lower-V bias for $x \leqslant 0.01$, indicating that excess current flows through the Schottky barrier. The hysteretic behavior appears only for the bias regions with excess current. The excess current increases for junctions with heavier doping, which have reduced barrier width, and hence can be attributed to a tunneling process. In the resistance switching process from the HRS to LRS, a large forward-bias voltage triggers an increase in the tunneling current.

B. *C-V* characteristics

The reverse-bias behavior of a Schottky junction can be well characterized by the *C-V* relationship given by

$$\frac{1}{C^2} = \frac{V_{bi} - V}{\varepsilon_0 \varepsilon_S S^2 N_D}, \tag{3}$$

where V_{bi} is the built-in potential voltage, ε_0 the dielectric constant of vacuum, ε_S the relative dielectric constant of the

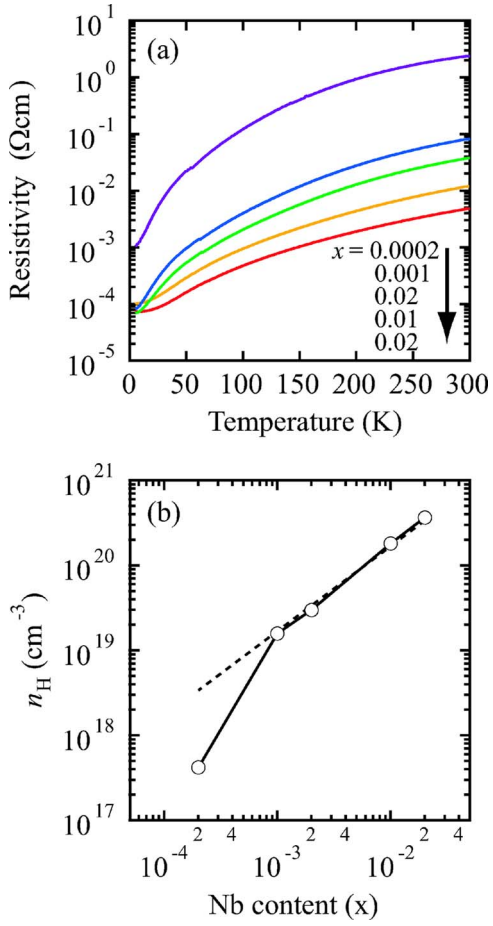

FIG. 4. (Color online) (a) Temperature dependence of resistivity for $SrTi_{1-x}Nb_xO_3$ (Nb:STO; x=0.0002, 0.001, 0.002, 0.01, and 0.02) single-crystal substrates. The metallic behaviors suggest that the Nb:STOs for all doping levels are degenerated semiconductors. (b) Actual electron concentration (n_H) evaluated from Hall measurement as a function of nominal Nb concentration (x), which was confirmed by inductively coupled plasma emission spectroscopy. In the most lightly doped sample with x=0.0002, more than 85% of the Nb dopant is inactive, whereas the samples with $x \geqslant 0.001$ show almost 100% activation of carriers.

depletion layer, and N_D the ionized donor concentration in the depletion layer.[29] Figure 3 shows $1/C^2$-V characteristics of the junctions for $x \leqslant 0.01$. Because of the large leakage current under reverse bias, reliable C-V characteristics could not be measured for the x=0.02 junction. The relationship shows a straight line, as expected from Eq. (3). A slight deviation appears at high V for heavily doped samples, possibly due to the electric-field dependence of ε_S for Nb:STO, as well as to the leakage current (see Fig. 2). One can extract $\varepsilon_S N_D$ and V_{bi} from the slope of straight lines in the lower bias region and from the intersection of V at $1/C^2$=0, respectively. From the doping level dependence of these values, as well as n and ϕ_B obtained from the I-V characteristics, we can deduce the potential profile of the Schottky barrier and its dependence on the Nb-doping level.

To discuss the doping level dependence of these values, we first evaluated the effective Nb concentration that can produce carrier electrons in the conduction band. As seen in

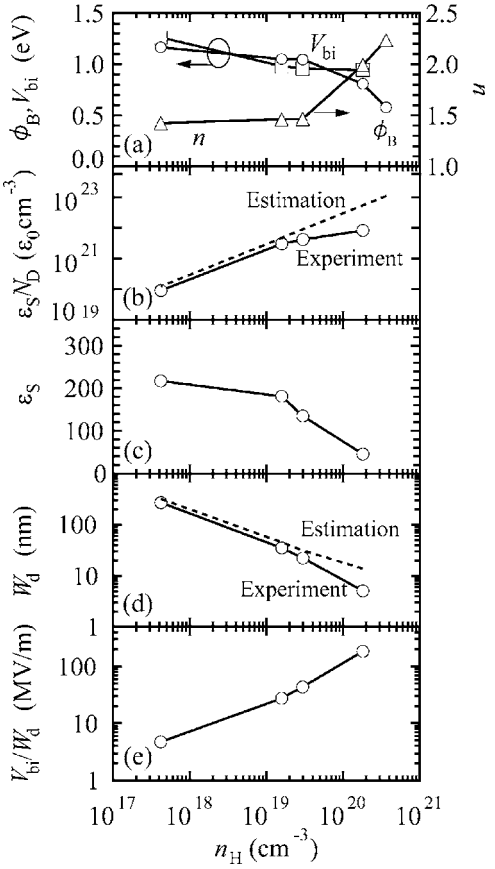

FIG. 5. Electron concentration n_H dependence of (a) V_{bi}, ϕ_B, and n, (b) $\varepsilon_S N_D$, (c) ε_S, (d) W_d, and (e) V_{bi}/W_d. The dotted lines in (b) and (d) represent the estimated value, assuming ε_S to be 300, independent of n_H, which corresponds to the value of undoped $SrTiO_3$ at room temperature.

Fig. 4(a), the temperature dependence of the resistivity for all of the Nb:STO substrates shows a metallic behavior. This means that the Nb:STO substrates for all doping levels are degenerated semiconductors and the Fermi level locates above the bottom of the conduction band. For a degenerated semiconductor, the carrier concentration can represent the effective dopant concentration. Figure 4(b) shows the Hall concentration n_H versus the doping level x for Nb:STO. The dotted line represents the estimated n_H, assuming each Nb atom produces one electron. For $x \geqslant 0.001$, the measured n_H values coincide with the estimated ones within the precision of the measurements. However, the measured n_H is about 1/8 of the estimated one for the x=0.0002 sample, indicating that more than 85% of the Nb dopant is inactive. Since the effective Nb concentration in the most lightly doped sample is much smaller than the nominal one, the n_H value is used instead of the nominal doping level x, hereafter.

In Fig. 5(a), we plot V_{bi} evaluated from the C-V characteristics and ϕ_B and n evaluated from the I-V characteristics, as a function of n_H. As n_H increases, both V_{bi} and ϕ_B decrease. In a normal n-type semiconductor in which the Fermi level locates below the bottom of the conduction band, the Fermi level shifts upward with increasing donor concentration, resulting in an increase of V_{bi} in a Schottky junction. In a degenerated semiconductor, however, the Fermi level shifts

downward and the electron affinity increases with increasing doping level due to the band-gap narrowing effect.[30] For a Schottky junction consisting of a degenerated semiconductor, like the SRO/Nb:STO junctions in this study, V_{bi} and ϕ_B are thus expected to decrease as the doping level increases. This is in agreement with our observations. Figure 5(b) shows the n_H dependence of $\varepsilon_S N_D$ derived from C-V measurements. The dotted line represents the estimated value, assuming that ε_S is 300, independent of x, which is the value of undoped bulk STO at room temperature. In the more heavily doped region, the measured $\varepsilon_S N_D$ is much smaller than the estimated one. This result suggests that ε_S at the heavier doping is much smaller than that of the undoped STO. By replacing N_D with n_H as discussed above, we deduce the n_H dependence of ε_S, as plotted in Fig. 5(c). Here, ε_S decreases with increasing n_H and is close to 50 at $n_H \sim 2\times10^{20}$ cm^{-3} (x=0.01). This reduction of ε_S can be explained by the electric-field (E) dependence of ε_S. It is well known that undoped STO is quantum paraelectric and that at low temperatures its dielectric constant decreases as the electric field is increased.[31,32] For the Nb:STO case, Yamamoto *et al.*[33] evaluated the electric-field dependence of ε_S using $Ba_{1-x}K_xBiO_3$/Nb:STO (x=0.0002, 0.001, and 0.01) Schottky junctions. Since the width of the Schottky barrier (depletion layer) is much smaller than the thickness of bulk single-crystal STO, a very high electric field can be applied to the Schottky barrier. This enabled them to evaluate the electric-field dependence of ε_S in a high-electric-field region, even at room temperature. They found that the electric-field dependence of ε_S can be approximated by

$$\varepsilon_S(T,E) = \frac{b(T)}{\sqrt{a(T)+E^2}}, \tag{4}$$

where $a(T)$ and $b(T)$ are temperature-dependent constant and coefficient, having room-temperature values of 1.64×10^{15} V^2/m^2 and 1.48×10^{10} V/m, respectively.[33] According to the Schottky model, the depletion layer width is expressed as

$$W_d = \sqrt{\frac{2\varepsilon_0\varepsilon_S(V_{bi}-V)}{eN_D}}. \tag{5}$$

From this equation and the slope of $1/C^2$-V curves, W_d of the SRO/Nb:STO junctions at V=0 can be estimated, and the n_H dependence of W_d is shown in Fig. 5(d). Here, if we consider V_{bi}/W_d as the average electric field E_S built into the depletion layer of the SRO/Nb:STO junctions, E_S is estimated to be higher than 200 MV/m for the x=0.01 junction ($n_H \sim 2\times10^{20}$ cm^{-3}), as shown in Fig. 5(e). From Eq. (4), we can estimate $\varepsilon_S \sim 73$ when an electric field E of 200 MV/m is applied to Nb:STO. This value is close to the evaluated value of $\varepsilon_S \sim 50$ of the x=0.01 junction.

C. Model of CER effect

Except for the hysteretic behavior, the rectifying I-V characteristics of the SRO/Nb:STO junctions agree with those expected for a conventional n-type semiconductor Schottky junction. Considering the band-gap narrowing effect and the

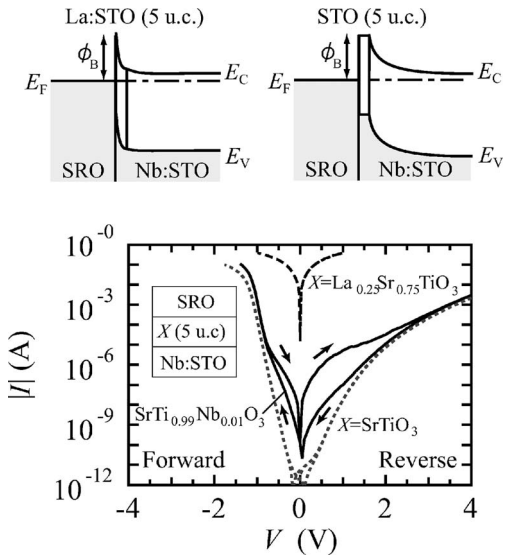

FIG. 6. I-V characteristics of the interface-engineered $SrRuO_3/X$ (2 nm)/$SrTi_{1-x}Nb_xO_3$ (x=0.01) junctions, where X=pristine $SrTiO_3$ (a band insulator) and $Sr_{0.75}La_{0.25}TiO_3$ [a metal whose carrier number is much larger than Nb:STO (Ref. 34)]. The CER effect is completely absent in these interface-engineered junctions.

electric-field dependence of ε_S for Nb:STO, the doping level dependence of the C-V characteristics can also be discussed in the framework of a conventional semiconductor Schottky junction. Here, we should note that no hysteretic behavior is observed in the C-V characteristics, unlike in the I-V characteristics. This suggests that the potential profile of the Schottky barrier remains almost unchanged between the HRS and LRS. According to analyses of the hysteretic I-V characteristics under forward bias, the tunneling current dominates in the LRS. Based on these experimental results, we can devise the following model of the CER effect for the heteroepitaxial Schottky junctions. In the Schottky barrier, there exist trapping states, such as impurity states and defects. When a large forward-bias voltage is applied to the Schottky junction, electrons are discharged from the trapping states, resulting in unoccupied trapping states in the Schottky barrier. In the lower-bias-voltage region, electrons can resonantly tunnel through the Schottky barrier using these unoccupied trapping states. When a large reverse-bias voltage is applied, electrons are captured in the trapping states, resulting in the closure of the resonant tunneling paths.

In this model, the CER properties may depend on the trapping state density in the vicinity of the interface and on the thickness of the Schottky barrier. To examine this assumption, we investigated the I-V characteristics of the SRO/Nb:STO (x=0.01) junctions, in which the doping level at the interface was intentionally changed. To modify the doping level at the interface, we prepared interface-engineered SRO/X (2 nm)/Nb:STO junctions, where X is either undoped STO or very heavily electron-doped $La_{0.25}Sr_{0.75}TiO_3$ (La:STO, corresponding to x=0.25). The substitution of La^{3+} for Sr^{2+} can more effectively provide electrons into the conduction band as compared to the substitution of Nb^{5+} for Ti^{4+}.[34] As shown in Fig. 6, the SRO/STO/Nb:STO junction

remains, showing a rectifying *I-V* characteristic, but the hysteretic behavior, i.e., the CER effect, disappears. This suggests that the 2-nm-thick STO layer prevents the formation of the resonant tunneling paths. The band diagram of the SRO/STO/Nb:STO junction is schematically shown in the illustrations at the top of Fig. 6. Because there is no dopant in the STO layer, there are very few impurity states which host the resonant tunneling. On the other hand, the SRO/La:STO/Nb:STO junction shows a quasi-Ohmic behavior and no CER effect. Because the SRO/La:STO/Nb:STO can be regarded as a metal/$n+$/n junction, the Schottky barrier width in the vicinity of the interface is reduced, as shown in the illustrations at the top of Fig. 6. Thus, electrons possibly pass through the thin Schottky barrier via a direct tunneling process. It is noted that when X=Nb:STO (x=0.01) was inserted as a homoepitaxial film, the observed CER effect was similar to that in SRO/Nb:STO (x=0.01) junction. These results suggest that the presence of the CER effect requires an appropriate doping level which can provide an adequate density of impurity states and thickness of the Schottky barrier for resonant tunneling.

IV. CONCLUSIONS

We have demonstrated a colossal electroresistance (CER) effect at the heteroepitaxial interface of $SrRuO_3/SrTi_{1-x}Nb_xO_3$ Schottky junctions with various doping levels x=0.0002–0.002. The rectifying *I-V* and *C-V* characteristics of the junctions agree with those expected for a conventional *n*-type semiconductor Schottky junction. The junctions with x=0.0002–0.01 show hysteretic *I-V* characteristics due to the CER effect, where forward (reverse) bias stress reduces (enhances) the junction resistance. The x dependence of the CER properties and the absence of hysteresis in the *C-V* characteristics suggest that the resistance switching in the Schottky junction results from the change in conductance through additional resonant tunneling paths rather than a change in the barrier potential profile.

ACKNOWLEDGMENTS

The authors would like to thank I. H. Inoue, T. Oka, N. Nagaosa, Y. Ogimoto, and Y. Tamai for useful discussions. This work was supported in part by the Industrial Technology Research Grant Program in 2005 from the New Energy and Industrial Technology Development Organization (NEDO) of Japan.

*Author to whom correspondence should be addressed; electronic address: a.sawa@aist.go.jp

[1] M. Imada, A. Fujimori, and Y. Tokura, Rev. Mod. Phys. **70**, 1039 (1998).
[2] A. Beck, J. G. Bednorz, Ch. Gerber, C. Rossel, and D. Widmer, Appl. Phys. Lett. **77**, 139 (2000).
[3] Y. Watanabe, J. G. Bednorz, A. Bietsch, Ch. Gerber, D. Widmer, A. Beck, and. S. J. Wind, Appl. Phys. Lett. **78**, 3738 (2001).
[4] S. Q. Liu, N. J. Wu, and A. Ignatiev, Appl. Phys. Lett. **76**, 2749 (2000).
[5] W. W. Zhuang, W. Pan, B. D. Ulrich, J. J. Lee, L. Stecker, A. Burmaster, D. R. Evans, S. T. Hsu, M. Tajiri, A. Shimaoka, K. Inoue, T. Naka, N. Awaya, K. Sakiyama, Y. Wang, S. Q. Liu, N. J. Wu, and A. Ignatiev, Tech. Dig. - Int. Electron Devices Meet. **2002**, 193.
[6] I. G. Baek, M. S. Lee, S. Seo, M. J. Lee, D. H. Seo, D.-S. Suh, J. C. Park, S. O. Park, H. S. Kim, I. K. Yoo, U.-In Chung, and J. T. Moon, Tech. Dig. - Int. Electron Devices Meet. **2004**, 587.
[7] A. Chen, S. Haddad, Y. C. Wu, T. N. Fang, Z. Lan, S. Avanzino, S. Pangrle, M. Buynoski, M. Rathor, W. Cai, N. Tripsas, C. Bill, M. VanBuskirk, and M. Taguchi, Tech. Dig. - Int. Electron Devices Meet. **2005**, 765.
[8] A. Baikalov, Y. Q. Wang, B. Shen, B. Lorenz, S. Tsui, Y. Y. Sun, Y. Y. Xue, and C. W. Chu, Appl. Phys. Lett. **83**, 957 (2003).
[9] S. Tsui, A. Baikalov, J. Cmaidlka, Y. Y. Sun, Y. Q. Wang, Y. Y. Xue, C. W. Chu, L. Chen, and J. Jacobson, Appl. Phys. Lett. **85**, 317 (2004).
[10] A. Sawa, T. Fujii, M. Kawasaki, and Y. Tokura, Appl. Phys. Lett. **85**, 4073 (2004).
[11] T. Fujii, M. Kawasaki, A. Sawa, H. Akoh, Y. Kawazoe, and Y. Tokura, Appl. Phys. Lett. **86**, 012107 (2005).
[12] A. Sawa, T. Fujii, M. Kawasaki, and Y. Tokura, Jpn. J. Appl. Phys., Part 2 **44**, L1241 (2005).
[13] Y. Tokunaga, Y. Kaneko, J. P. He, T. Arima, A. Sawa, T. Fujii, M. Kawasaki, and Y. Tokura, Appl. Phys. Lett. **88**, 223507 (2006).
[14] A. Sawa, T. Fujii, M. Kawasaki, and Y. Tokura, Appl. Phys. Lett. **88**, 232112 (2006).
[15] H. Sim, H. Choi, D. Lee, M. Chang, D. Choi, Y. Son, E. H. Lee, W. Kim, Y. Park, I. K. Yoo, and H. Hwang, Tech. Dig. - Int. Electron Devices Meet. **2005**, 777.
[16] S. Seo, M. J. Lee, D. H. Seo, S. K. Choi, D.-S. Suh, Y. S. Joung, I. K. Yoo, I. S. Byun, I. R. Hwang, S. H. Kim, and B. H. Park, Appl. Phys. Lett. **86**, 093509 (2005).
[17] D. C. Kim, S. Seo, S. E. Ahn, D.-S. Suh, M. J. Lee, B.-H. Park, I. K. Yoo, I. G. Beak, H.-J. Kim, E. K. Yim, J. E. Lee, S. O. Park, H. S. Kim, U-In Chung, J. T. Moon, and B. I. Ryu, Appl. Phys. Lett. **88**, 202102 (2006).
[18] B. J. Choi, D. S. Jeong, S. K. Kim, C. Rohde, S. Choi, J. H. Oh, H. J. Kim, C. S. Hwang, K. Szot, R. Waser, B. Reichenberg, and S. Tiedke, J. Appl. Phys. **98**, 033715 (2005).
[19] I. H. Inoue, M. J. Rozenberg, S. Yasuda, M. J. Sànchez, M. Yamazaki, T. Manago, H. Akinaga, H. Takagi, H. Akoh, and Y. Tokura, Proceedings of the IEEE Non-Volatile Memory Technology Symposium Houston, 2005, p. 131.
[20] K. Kinoshita, T. Tamura, H. Aso, H. Noshiro, C. Yoshida, M. Aoki, Y. Sugiyama, and H. Tanaka, Proceedings of the IEEE Non-Volatile Semiconductor Memory Workshop Monterey, 2006, p. 84.
[21] Z. Szot, W. Speier, G. Bihlmayer, and R. Waser, Nat. Mater. **5**, 312 (2006).
[22] X. Chen, N. J. Wu, J. Strozier, and A. Ignatiev, Appl. Phys. Lett. **87**, 233506 (2005).

[23] T. Oka and N. Nagaosa, Phys. Rev. Lett. **95**, 266403 (2005).
[24] M. J. Rozenberg, I. H. Inoue, and M. J. Sànchez, Phys. Rev. Lett. **92**, 178302 (2004).
[25] M. J. Rozenberg, I. H. Inoue, and M. J. Sànchez, Appl. Phys. Lett. **88**, 033510 (2006).
[26] A. Odagawa, H. Sato, I. H. Inoue, H. Akoh, M. Kawasaki, Y. Tokura, T. Kanno, and H. Adachi, Phys. Rev. B **70**, 224403 (2004).
[27] K. Aoyama, K. Waku, A. Asanuma, Y. Uesu, and T. Katsufuji, Appl. Phys. Lett. **85**, 1208 (2004).
[28] K. S. Takahashi, A. Sawa, Y. Ishii, H. Akoh, M. Kawasaki, and Y. Tokura, Phys. Rev. B **67**, 094413 (2003).
[29] S. M. Sze, *Physics of Semiconductor Devices*, 2nd ed. (Wiley, New York, 1981).
[30] S. M. Sze, *Semiconductor Devices, Physics and Technology*, 2nd ed. (Wiley, New York, 2001).
[31] E. Sawaguchi, A. Kikuchi, and Y. Kodera, J. Phys. Soc. Jpn. **17**, 1666 (1962).
[32] M. A. Saifi and L. E. Cross, Phys. Rev. B **2**, 677 (1970).
[33] T. Yamamoto, S. Suzuki, H. Suzuki, K. Kawaguchi, K. Takahashi, and Y. Yoshisato, Jpn. J. Appl. Phys., Part 2 **36**, L390 (1997); T. Yamamoto, S. Suzuki, K. Kawaguchi, and K. Takahashi, Jpn. J. Appl. Phys., Part 1 **37**, 4737 (1998).
[34] Y. Tokura, Y. Taguchi, Y. Okada, Y. Fujishima, T. Arima, K. Kumagai, and Y. Iye, Phys. Rev. Lett. **70**, 2126 (1993).